Structural and electronic properties of U_4O_9 from *ab initio* and empirical potential calculations

Jean-Paul Crocombette, Orane Barbour, and Fabien Bruneval
Université Paris-Saclay, CEA, Service de Corrosion et de Comportement des Matériaux, SRMP, 91191 Gif-sur-Yvette, France

(Received 3 April 2023; accepted 1 June 2023; published 22 June 2023)

We address here the description of the different phases of U_4O_9 with *ab initio* density functional theory and molecular dynamics empirical potential calculations. These phases are built from the UO_2 fluorite by the addition of oxygen interstitials which assemble in clusters named cuboctahedra. Due to the unit cell size and complexity, their simulation represents a formidable task for numerical approaches. With DFT+U, we study in detail two potential structures for $\alpha-U_4O_9$, however, these are just two representatives among the numerous coexisting structures we found. The role of the different valence uraniums (U^{4+}, U^{5+}, and possibly U^{6+}) is highlighted thanks to our quantum-mechanical approach. Temperature effects are then appraised with empirical potentials to describe the evolution of the U_4O_9 structure with temperature. We observe a continuous symmetrization of the structure with increasing temperature. Indeed, below 800 K, it gradually turns cubic and the cuboctahedral oxygen clusters tend to symmetrize. Beyond 800 K, the cuboctahedra start to disappear up to 1400 K, where none can be found in our simulated structures.

DOI: 10.1103/PhysRevMaterials.7.063602

I. INTRODUCTION

Uranium oxide exists in several forms, the most important one being UO_2, the main component of standard nuclear fuel. The first overstoichiometric oxide is U_4O_9, which shares with UO_2 the face-centered cubic arrangements of uranium atoms. The overstoichiometry is accommodated by the incorporation of oxygen interstitials in the UO_2 fluorite structure. These interstitials gather in clusters containing five interstitials, noted I^5. They were originally thought to be filled symmetric cuboctahedra [1] (I^5_C): each I^5_C is made of 12 oxygen atoms forming the cuboctahedron *per se*, plus an additional oxygen interstitial in its center. The I^5_C are positioned around an interstitial site in the fluorite structure and replace an eight-oxygen atom cube. They thus count as five oxygen interstitials, which explains the I^5 notation. Three phases of U_4O_9 have been observed experimentally [2–4] with increasing temperature. All phases have 424 atoms in their body-centered unit cell. Their exact stoichiometry is therefore $U_{128}O_{286}$ or $UO_{2.234375}$. I^5 clusters exhibit a specific order with $1/2\langle 321\rangle$ vector types for I^5-I^5 first distance. The structure is best visualized in the 828 conventional cubic cell, which corresponds to a $4 \times 4 \times 4$ repetition of the conventional cubic cell of UO_2.

The β phase is observed at intermediate temperatures (between 340 and 820 K). Its structure has been well characterized by Willis and coworkers and others [1,5,6]. It exhibits the $I4\bar{3}d$ space group and I^5 clusters prove distorted and shifted. Above 820 K, U_4O_9 adopts the so-called γ phase that is isosymmetric to the β phase, but with variations in some interatomic distances [7]. This defined phase dissolves into the high-temperature UO_{2+x} solid solution above 1400 K.

The α phase is stable below 340 K. It has a lower symmetry space group: $R3c$ [7,8]. The α phase has been much less characterized than the β phase. We have recently proposed descriptions of its atomic structure based on atomistic simulations with a semiempirical potential. The lowest energy structure proves orthorhombic, in disagreement with experiments. The next phase up in energy (1.2 eV per U_4O_9 unitcell, i.e., 2.9 meV per atom) is rhombohedral as in experiments. This rhombohedral structure has the correct $R3c$ space group. In both structures, I^5 clusters adopt a specific structure I^5_{CX}, which lie in between I^5_C and I^5_X (see below).

Starting from the rhombohedral structure, we performed Rietveld refinement of neutron diffraction experiments and obtained a reasonable fit at the expense of noticeable shifts of the atomic positions. We thus proposed three different structures: two from simulations and one from experiments.

Attempts have been made [9] using more accurate description of atomic interactions, namely, density functional theory (DFT) to deduce the structure of I^5 clusters in U_4O_9 from the study of the structure of isolated clusters of oxygen interstitial in UO_2. That proved an uneasy task. Indeed, DFT calculations on actinide oxides are not straightforward and heavy computationally. For many years, these calculations pointed to the stability of the I^4_X cluster (made of four oxygen interstitials) as more stable than any form of I^5. This appears to be due to spurious interactions between defects due to too-small interaction boxes, as suggested by empirical potentials [8] and recently confirmed by DFT (see Yang and Wirth [10]). These authors did find that I^5 clusters are the most stable arrangements of oxygen interstitials in UO_2. However, the clusters adopt a so-called I^5_X structure quite different from symmetrical cuboctahedra as the five interstitials are packed with the four oxygens, forming the regular face of the fluorite oxygen cube.

The exact atomic structure of U_4O_9, especially the one of I^5, thus remains unclear, especially in the α phase. Moreover, the evolution of U_4O_9 with increasing temperature with atomistic simulations requires study. In the present paper, we use atomic scale simulations, using two complementary approaches, to tackle these two points.

We first present results of DFT calculations of the structure of U_4O_9. We took extra care to describe in the best possible way the electronic structure of the material. We present our prediction of the structure of U_4O_9 at 0 K.

We complement this study by semiempirical potential simulations of the evolution of the structure of I^5 clusters in U_4O_9 with increasing temperature, which we connect with experimental observations available in literature.

II. *AB INITIO* $\alpha-U_4O_9$ AT 0 K

A. DFT+U calculations

The electronic structure calculations in UO_2 are a delicate matter, mostly because of the localized open-shell f electrons of uranium. To address this problem, the DFT+U [11,12] is today the most used approach: it is very cost effective (it is a standard mean-field approach) and yields sensible physical results (it opens up a band gap in Mott insulators), however, at the price of introducing empirical on-site electron interaction parameters U and J. While U and J could, in principle, be calculated [13–15], in the present paper, we simply adjusted the parameters to obtain band gaps and the lattice constant of UO_2 in correct agreement with experiment.

Here we use the rotationally invariant formulation of Liechtenstein *et al.* [11] as implemented in VASP [16] together with the PBE functional [17]. We use noncollinear magnetism (with transverse 3**k** ordering) and introduce the spin-orbit coupling. With these two contributions, the unit cell of UO_2 remains cubic, as it should in the experiment. In our previous calculations without these effects [18], the UO_2 unit cell experienced a slight tetragonal distortion.

The inclusion of the experimental magnetic order has a very mild effect (if any) on the energetic defects we are interested in in this paper. Notice the very small energy scale reported in Ref. [19]. Quite the opposite, the inclusion of spin-orbit coupling has a very positive consequence on our calculations: the infamous multiple minima problem that affects DFT+U calculations during the electronic self-consistent cycles (see Refs. [20,21]) is much mitigated, as also noticed by Yang and Wirth [10]. Our hand-waving interpretation is that the $L \cdot S$ spin-orbit term is a strong driving term that allows the minimization algorithm to overcome the problematic barriers separating the local minima of DFT+U. That is why we do not employ any advanced technology and rely on the default algorithm in contrast to our previous studies [18,22].

Summarizing the electronic structure parameters of this paper, we use $U = 3.70$ eV, $J = 0.51$ eV for uranium f electrons, a plane-wave cutoff of 500 eV, and uranium projector-augmented wave pseudopotential [23] with 14 electrons. The k-point sampling is limited to the sole Γ-point, since we only consider large cells here with 108 or 128 formula units of UO_2. Notice that the U had to be reduced compared to that of calculations without spin-orbit coupling. With these settings, the UO_2 lattice constant is 5.537 Å (experimental value is 5.47 Å [24]) and the band gap is 2.36 eV (optical experimental value is 2.1 eV [25]).

TABLE I. DFT+U clustering energies (eV) of the oxygen clusters in UO_2 and U_4O_9.

Cluster type	UO_2 This paper	UO_2 Yang-Wirth [10]	U_4O_9 This paper
I^1_O	0.00	0.00	
I^4_X	−0.50	−0.54	−0.62
I^5_C	−0.49		−0.67
I^5_{CX}	−0.54		−0.60
I^5_X	−0.55	−0.67	−0.70

B. Isolated oxygen clusters in UO_2

Before addressing U_4O_9 that is built from periodically spaced oxygen clusters, we investigate these oxygen clusters as isolated objects in the perfect UO_2 matrix first.

To evaluate quantitatively, the formation of oxygen defects in the UO_2 host, we use the clustering energy per oxygen atom E_c:

$$E_c(I^n) = \frac{1}{n}\left[E(I^n) + (n-1)E(\varnothing) - nE\left(I^1_O\right)\right], \qquad (1)$$

where $E(I^n)$ stands for the total energy of the supercell containing one oxygen cluster I^n, $E(\varnothing)$ for the perfect supercell of the same size with no cluster, and $E(I^1_O)$ for the same supercell with a single isolated interstitial I^1_O.

The clustering energy measures the energy gained when forming clusters as compared to isolated interstitial I^1_O. At variance with the formation energies often used to characterize defect energetics, the cluster energy is intrinsic to the bulk material and does not need any reference to an external chemical potential, as can be observed in Eq. (1).

In this paper, we employ a $3 \times 3 \times 3$ cubic supercell, which translates into a host of 108 U and 216 O. We follow Yang and Wirth [10] who concluded that the smaller $2 \times 2 \times 2$ supercells are not sufficiently large to extract the isolated clustering energies. Targeting the U_4O_9 structure, we limit our study to neutral oxygen clusters, since in U_4O_9 charge neutrality will eventually enforce this balance.

Besides the isolated single oxygen interstitial I^1_O, we study four different I^5 oxygen clusters that are drawn in Fig. 1: the I^4_X proposed by Andersson *et al.* [9]; the I^5_C cuboctahedron extracted from Bevan *et al.* U_4O_9 structure [1]; the I^5_{CX} twisted cuboctahedron obtained from SMTB-Q empirical potential by Soulié *et al.* [8]; and the I^5_X half cuboctahedron calculated by Yang and Wirth [10].

The clustering energies of these four clusters are reported in Table I. Our energies compare favorably with the Yang and Wirth results when available. While the I^5_X cluster prevails in terms of energy, it should be noted that all these energies span a narrow range. An interesting feature is the displacement of the central oxygen atom in I^5_C. In contrast with the experimental position in U_4O_9 determined by Cooper and Willis [5], which found a ⟨111⟩ shift, the DFT+U calculations favor a ⟨110⟩ shift.

In the DFT+U, we are able to identify the uranium cations that switch valence from U^{4+} in UO_2 to U^{5+} or even U^{6+} to compensate for the additional oxygen interstitial that formally bear a −2 charge state. Based on calculations for U_3O_8

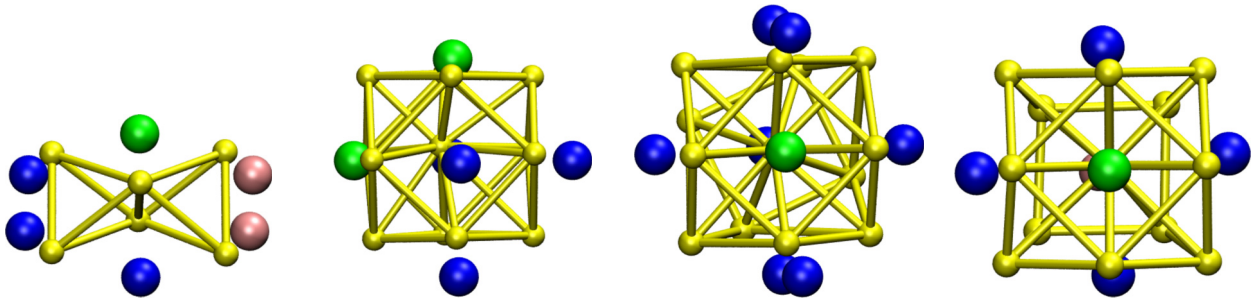

FIG. 1. Oxygen cluster structures with their uranium first neighbors. From left to right, the clusters are I^4_X, I^5_C, I^5_{CX}, and I^5_X. These structures are the relaxed DFT+U positions. The yellow sticks and balls represent the oxygen atoms, whereas the large balls are the uranium atoms. Pink color stands for U^{4+}, blue for U^{5+}, and green for U^{6+}.

and the positive polaron in UO_2, we observed that the total charge obtained from atomic projections or the Bader vary by at most 0.2 electrons (as also reported in Ref. [26]) and are not conclusive enough to identify the uranium valence. The spin magnetization of each uranium appears as a rather reliable marker of the valence. But, surprisingl,y we remarked that the projection on the atomic Ud shell is an even more distinctive fingerprint of the uranium valence: U^{6+} valence induces a larger d occupation than U^{5+}, that in turn shows a larger d occupation than U^{4+}. With this technique, we report in Fig. 1 the valence of the uranium nearby an oxygen cluster. We observe the occurrence of U^{6+} in the four clusters. In all the calculations we have carried out, we always have found the ideal number of U^{5+} and U^{6+} cations to compensate the oxygen negative charges. This fact gives us confidence in our detection procedure of U^{5+} and U^{6+}. As expected in a Mott insulator, no delocalized electron or hole is created in the band structure.

After this preliminary study on isolated oxygen clusters, we now turn to the crystalline $\alpha-U_4O_9$ phase based on periodic oxygen clusters.

C. $\alpha-U_4O_9$

We now explore the structure candidates for the $\alpha-U_4O_9$ based on DFT+U energies. This study had to face two main difficulties. First, the unit cell of U_4O_9 is very large: it contains 414 atoms, including 128 uranium atoms. This uncommon size rules out any systematic method such as those that are routinely employed in crystal structure prediction [27]. The computational tasks would be orders of magnitude too large. Second, we found that the standard structural minimizations always end up in local energy minima, e.g., two similar guess structures often produce two distinct final structures, with two different energies.

Owing to these difficulties, we adopt an iterative strategy based on human-intuition-driven guesses. We have calculated 34 structure candidates, which includes the experimental structures published in Refs. [5,8] and the theoretical structure in Ref. [9]. The other candidate structures have been produced by placing the isolated oxygen clusters obtained in the previous section in the host atoms with the experimental positions of Cooper and Willis [5]. For the creation of the unit cell, we enforce the $R3c$ space group symmetries so once an oxygen cluster is inserted, the other five clusters are uniquely obtained by application of the space group operations. Different orientations of the clusters with respect to the host have been tried. Note that the position of the U^{5+} or U^{6+} cations are not preset: we let the electronic structure optimization localize the charge wherever it is energetically favorable. We experienced that simply tuning the oxygen environment is not sufficient to enforce the localization of a U^{5+} or U^{6+} valence.

In Fig. 2, we propose a classification of the 34 resulting U_4O_9 structures after structural optimization with DFT+U. Note that some structures are beyond the represented scale. We use the pair correlation function $g(r)$ to sort out the different U_4O_9 families. Indeed, the $g(r)$ is handy since it is insensitive to the orientation and to the origin of the crystal cell. Besides a few outliers, this two-dimensional representation correlates well with the type of oxygen clusters, as determined by direct observation. We have created two categories of I^5_C: those that were created out of experimental positions and those that were created from the isolated clusters presented above. This is not a surprise that the structure with $g(r)$ closest

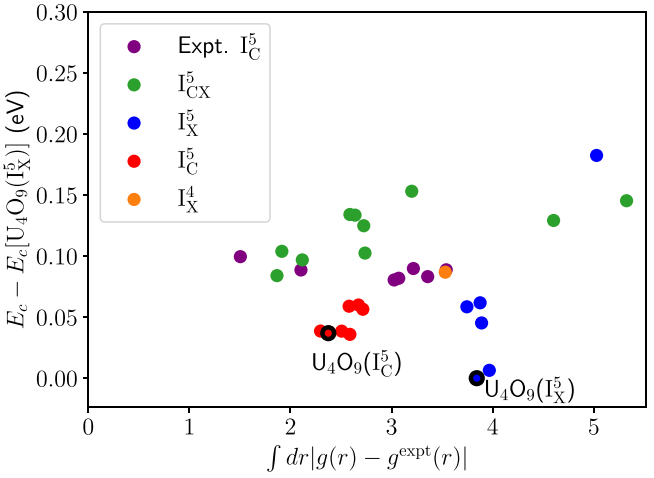

FIG. 2. Bidimensional scatter plot reporting the clustering energy E_c as a function of difference in the pair correlation function $g(r)$ in arbitrary units. The experimental $g(r)$ from Ref. [28] has been considered as the reference. The most stable DFT+U structure sets the zero of energies. The coloring scheme evidences the type of oxygen clusters that are present. Two structures $U_4O_9(I^5_X)$ and $U_4O_9(I^5_C)$ that will be studied in detail are highlighted with a black edge.

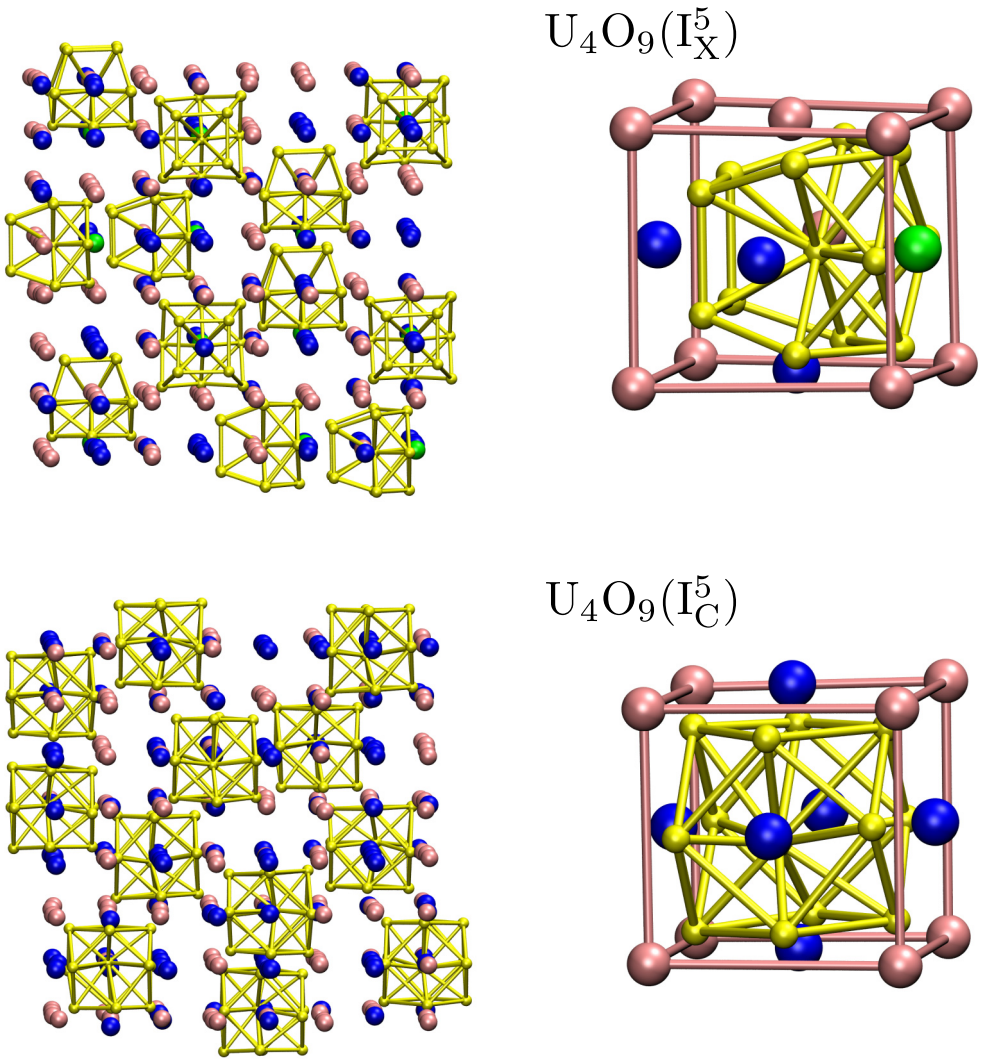

FIG. 3. Relaxed structures for the two candidates $U_4O_9(I^5_X)$ (upper panels) and $U_4O_9(I^5_C)$ (lower panels). On the left, we represent the conventional cell containing 12 clusters. On the right, we zoom in for a close-up view of a single oxygen cluster with its neighboring uranium atoms. The yellow sticks and balls represent the oxygen atoms, whereas the large balls are the uranium atoms. The regular fluorite oxygen atoms are not represented for visualization purposes. Pink color stands for U^{4+}, blue for U^{5+}, and green for U^{6+}.

to experiment is a relaxation starting from some experimental positions. We observe that the optimized DFT+U energies almost form a continuum. Structures containing the same type of clusters often end up with different energies because of local minimum trapping. The structure named I^4_X is interesting: it is the theoretical structure proposed by Andersson *et al.* [9], which is based on periodic I^4_X clusters in UO_2, however, with a completely different ordering and space-group than U_4O_9. This structure does not deviate so much from the experimental $g(r)$.

The best clustering energies for each cluster family is then reported in Table I. One notices that the I^5_{CX} cluster that was very competitive as an isolated specie, is not energetically favored in the U_4O_9 periodic structure.

Among those structures, we select two low-energy ones that will be representative of their respective family: the $U_4O_9(I^5_X)$ and the $U_4O_9(I^5_C)$ as highlighted in Fig. 2. The $U_4O_9(I^5_X)$ structure is our overall minimum in DFT+U energy but with a large $g(r)$ distance to experiment, whereas $U_4O_9(I^5_C)$ is more compatible with the experimental $g(r)$ but with a slightly higher energy. Both structures are drawn in Fig. 3 and their atomic positions and their pair correlation functions are reported as Supplemental Material [29].

$U_4O_9(I^5_X)$ is our best structure in terms of energy. It is constructed from I^5_X clusters. Before relaxation, the $R3c$ space-group symmetries were fulfilled, but then are broken in the final configuration. Attempts were made to symmetrize again the relaxed structure, but eventually yielding the broken-symmetry result. As drawn in the upper panels of Fig. 3, the nearest uranium atoms around the I^5_X assume U^{5+} valence for three of them, and U^{6+} for one of them. The rest of the U^{5+} are spread among the host uranium atoms. A detailed analysis of the pair correlation function (see Supplemental Material [29]) shows that U^{6+} correlates with shorter U–O bonds ($\sim$2.1 Å instead of $\sim$2.3 Å). However, XANES measurements advocate for the absence of U^{6+} in U_4O_9 [30,31], which raises some doubts about the actual existence of this DFT+U phase.

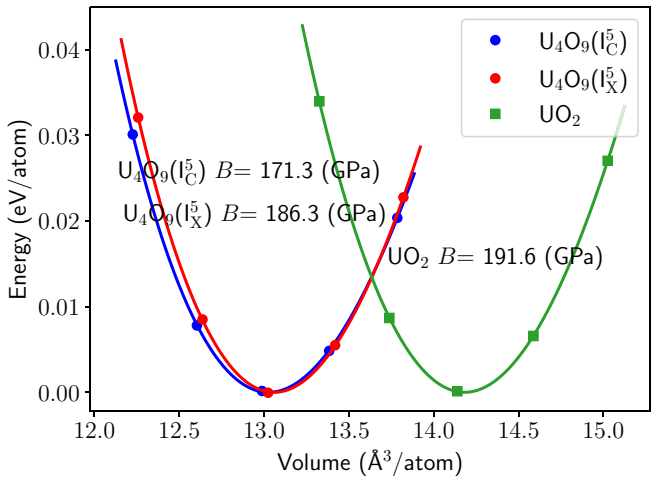

FIG. 4. Energy volume curve in eV/atom. The two U_4O_9 candidate structures are compared to plain UO_2. The minimum energy of each structure is set to zero. The bulk moduli B are given in GPa.

Our second interesting structure, $U_4O_9(I_C^5)$, is only 0.035 eV higher in terms of E_c. It is based on I_C^5, which are placed according to the $R3c$ space group. Symmetries are conserved all along with the relaxation. The oxygen charges are neutralized by U^{5+} valence only, as shown in the lower panels of Fig. 3. The six uranium atoms facing the I_C^5 clusters are all U^{5+} as hinted at in the neutron diffraction study by Desgranges *et al.* [7]. Note that uranium atoms in the corner of the cube containing the oxygen cluster are always U^{4+} for $U_4O_9(I_C^5)$ and $U_4O_9(I_X^5)$, which also agrees with Desgranges *et al.* [7].

Both structures have similar lattice vectors. The energy versus volume curves are shown in Fig. 4. For instance, in $U_4O_9(I_C^5)$, the lattice constant is 19.15 Å and the rhombohedral angle α is 109.61Å°, to be compared to 18.82 Å and α = 109.49Å° from neutron diffraction [8]. The lattice constant is slightly too long in DFT+U, however, it is already the case in plain UO_2. Then, it is more instructive to speak in terms of unit cell volume contraction. In DFT+U, this contraction amounts to 1%, whereas it is 2% in the experiment. Whereas the lattice are similar, the bulk moduli of $U_4O_9(I_X^5)$ and $U_4O_9(I_C^5)$ are rather different. Unfortunately, experimental values could not be found for U_4O_9.

We now turn to the electronic structure of U_4O_9, which is largely unknown in the experiment. Figure 5 reports the projected density-of-states for plain UO_2, $U_4O_9(I_X^5)$, and $U_4O_9(I_C^5)$. The overall total valence density of states is less structured in U_4O_9 than in UO_2, certainly due to the less ordered structure. The UO_2 band gap is 2.36 eV and is mostly due to U uranium atoms as expected for a Mott insulator. $U_4O_9(I_X^5)$ and $U_4O_9(I_C^5)$ have a much smaller band gap of 0.95 eV for both. This band gap narrowing is due to the introduction of the U^{5+}, which has a low-energy first empty state. In $U_4O_9(I_X^5)$, the U^{6+} atoms do not contribute to the band edges. The oxygen atoms belonging to the cluster have a vanishing spectral weight in the band gap region (not shown here). An experimental value of the fundamental band gap of U_4O_9 would be an important piece of information.

We further evaluated the cost of creating additional localized charges in $U_4O_9(I_C^5)$, or, in other words, of positive and negative polarons. Introducing a positive polaron amounts to turning one additional U^{4+} into U^{5+}. In DFT+U, the energy difference (including the monopole charge correction [32]) is 0.31 eV below the energy of a delocalized hole at the top valence band, which is a quite large energy gain. The creation of a negative polaron, (i.e., turning one U^{5+} into one U^{4+}) is even more favorable: the DFT+U energy is 0.57 eV below that of a delocalized electron at the bottom of the conduction band. These two polaron energies show that U^{4+} and U^{5+} valences easily switch in U_4O_9.

III. MOLECULAR DYNAMICS AT FINITE TEMPERATURE

The structure of U_4O_9 proves highly complex at zero temperature. In an attempt to study how this structure evolves with temperature, we switch to semiempirical potential molecular dynamics (MD) calculations. Indeed, *ab initio* (from DFT calculations) MD simulation are completely out of reach due to the unreasonable computer resources this would require.

A. Empirical potentials method

We use the second moment tight binding with charge equilibration potential (SMTB-Q) [33,34], with the same parametrization as in our previous studies on UO_2 and U_4O_9 at 0 K [8,22,35]. We start from two different structures: the lowest energy orthorombic one and the rhombohedral one just higher in energy. We considered also this second structure as

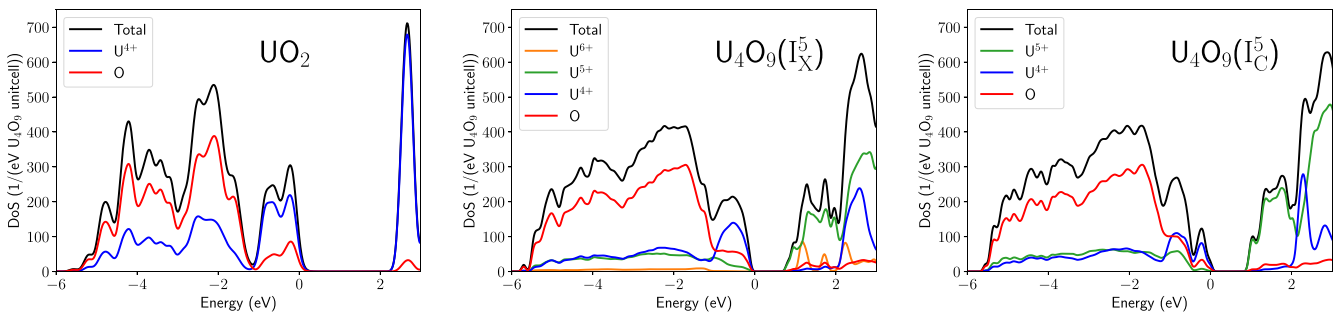

FIG. 5. Valence projected density of states of UO_2 (left-hand panel), $U_4O_9(I_X^5)$ (central panel), and $U_4O_9(I_C^5)$ (right-hand panel). The top valence energy has been set to zero. The UO_2 y axis is rescaled so to have the same number of uranium atoms as a U_4O_9 unit cell to ease the comparison.

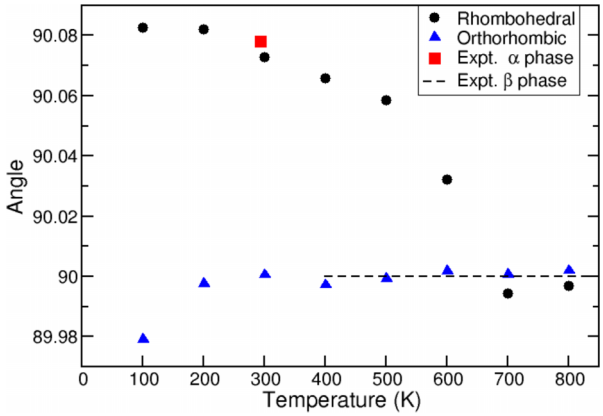

FIG. 6. Time-averaged cell angles as a function of temperature.

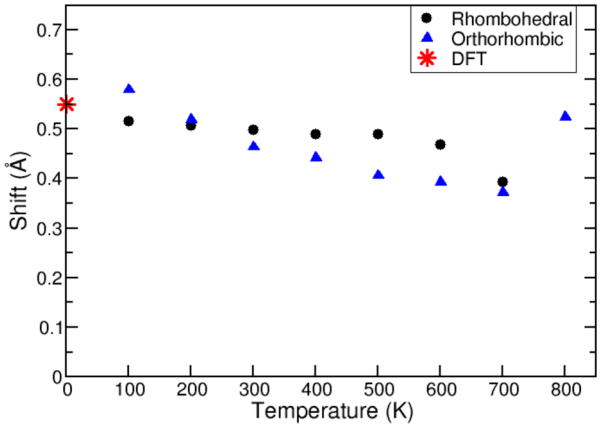

FIG. 7. Time-averaged shift of I^5 central atom with respect to the ideal interstitial site as a function of temperature.

it exhibits a closer agreement with available information from experiments (e.g., the correct space group). See our previous study for a detailed description of these two structures [8] at 0 K. We heat them by steps of 100 K up to 2000 K. We can thus compare the behaviors of these two structures with increasing temperature. We use a $2 \times 2 \times 2$ supercell of the conventional cubic cell of U_4O_9, which corresponds to 6624 atoms and originally 96 I^5_{CX}. The heating time is set to 50 ps. Then a constant temperature constant pressure run is performed for another 50 ps during which a snapshot of the atomic positions is stored every 0.5 ps. The atomic structure is analyzed for each of these snapshots and quantities are averaged over them.

B. Evolution of U_4O_9 structure with temperature

We first monitor the evolution of the cell angles (see Fig. 6). In the orthorhombic structure, the angles oscillate around 90° with temperature. More interestingly, for the rhombohedral structure, the angle proves to decrease with temperature from 90.08° at 100 K to 90° at 700 K. We also indicate the experimental value at room temperature obtained by Belbeoch *et al.* [2]. Our value proves strikingly close to this experimental value. Beyond 800 K, the angles simply oscillate around 90° (not shown in the figure). The transition to a perfectly (β-like) cubic structure is therefore slightly delayed in our calculations compared to experiments. The DFT value for the I^5_C rhombohedral structure is 90.3°, which deviates notably from both our empirical potential value and the experiment. The volume of the cell increases regularly temperature. However, one can note a noticeable increase of the thermal expansion coefficient from around 4d-6 K-1 to around 6d-6 K-1 between 900 K and 1200 K.

We find that whatever the starting structure, the uranium lattice is not affected by the heating up to the final 2000 K temperature. It remains face-centered cubic. Beyond thermal vibration and thermal expansion, no uranium atom was ever displaced during our simulations. The structural analysis can then be focused on the positions of the oxygen atoms and especially the one forming I^5 clusters. To detect them, we use a simple distance criterion, counting the number of oxygen atoms at the distance lower than 1.8 a_0 from empty cubes of the underlying fluorite structure (a_0 being the lattice parameter of the underlying fluorite structure at the considered temperature). If there are 13 oxygen atoms within the sphere, the defect is classified as a I^5. Eye inspection on some configurations confirms that this simple distance criterion indeed identifies the I^5. Other cubes may contain less than 13 but more than 8 oxygen ions. When such cubes are neighboring an I^5, they are just indicating the vicinity of the I^5 and do not contain any new defect. Otherwise, the detected cubes contain interstitial clusters of another type. These other defects prove short-lived and unstable, so they are not further characterized here.

While perfect cuboctahedra are symmetrical polyhedra, actual I^5 clusters are distorted. We follow the evolution of these distortions with temperature using two parameters. First, the oxygen interstitial inside the I^5 is not exactly at the center of the original eight-oxygen cube. For each of the 96 atoms inside the I^5 clusters, we monitor the vectorial shift of their actual position with respect to the center of the perfect cube and average this vector over the one hundred positions saved during each constant temperature run. We then calculate the average over all I^5 clusters in the box of the norm of these time averaged shifts. Second, due to the I^5 distortions, the distances between the atoms at the 12 vertices of the cuboctahedron and the internal atom are all different, while they would be equal if the clusters were perfectly symmetric. For each temperature, we calculated the average of each one of these distances along the one hundred snapshots.

Note that our empirical potentials, while quite accurate, fail to reproduce the exact structure of the $U_4O_9(I^5_C)$ DFT phase. But the magnitude of the shift and the dispersion of distances at 0 K with SMTB-Q are comparable in intensity to the ones of the DFT $U_4O_9(I^5_C)$ structure which is reassuring for our results, as we describe below.

We first present the results about the shift of the center of the I^5 with respect the center of the fluorite oxygen cube (see Fig. 7). The empirical potential values at low temperature prove very close to the DFT $U_4O_9(I^5_C)$ structure. Globally speaking, one can note that there is a partial centering of the central oxygen atom with increasing temperature. This centering is more pronounced in the orthorombic structure but can also be seen in the rhombohedral one. Starting at

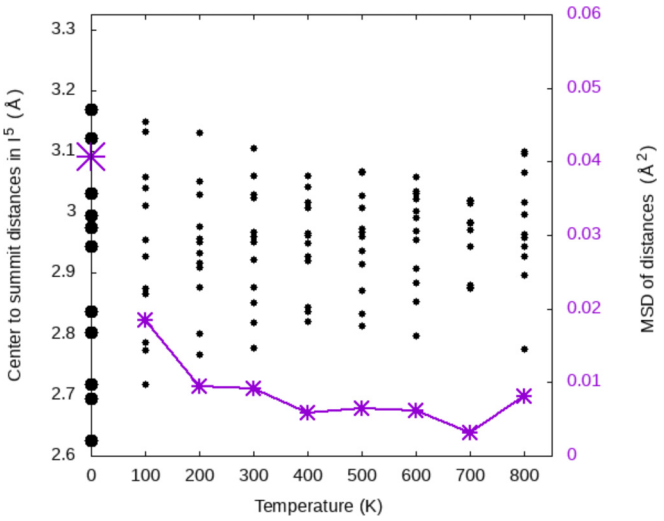

FIG. 8. Time-averaged distances between cuboctahedral atoms and the atom at the center of I^5 as a function of temperature and corresponding Mean Square Deviation. The values at 0 K are those of the I^5_C DFT structure.

800 K, the shift starts to increase again. This happens at the temperature where the I^5 clusters start to disappear during the simulation (see below).

The evolution of the average I^5 interatomic distances is exemplified in Fig. 8 in the case of one I^5 in the orthorhombic structure. The spread of distances tend to decrease upon heating from 0 K up to 700 K. This signals the symmetrization of the clusters with temperature. Starting at 800 K, some distances tend to deviate again from the average. These analyses cannot be pursued at higher temperatures because then I^5 clusters tend to disappear. The behavior proves very similar for all I^5 clusters in both structures.

Figure 9 indicates the average number of I^5 detected during each constant temperature runs in the orthorhombic structure (the behavior being very similar in the rhombohedric one). Below 800 K, all clusters remain in their original positions.

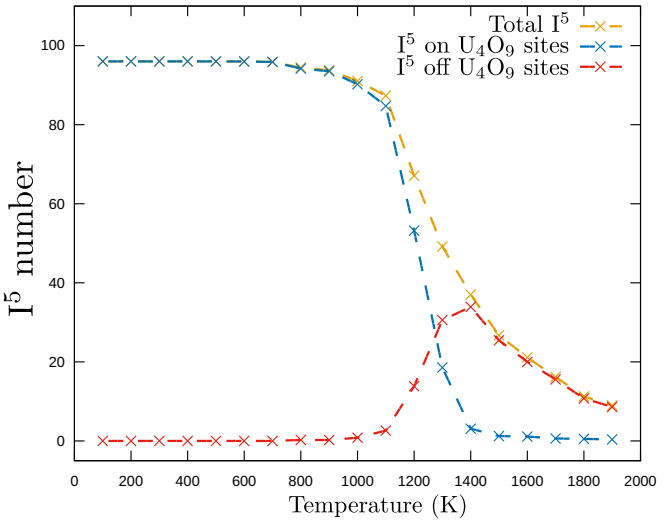

FIG. 9. Average number of detected number of I^5.

Then two types of I^5 clusters are observed: the ones that are situated on regular U_4O_9 sites, and the ones that appear centered on other interstitial sites. One can see that the number of I^5 clusters on the U_4O_9 sites rapidly goes down to zero between 900 K and 1400 K. This decrease in the number of I^5 clusters appears concomitant with the observed change in thermal expansion (see before). I^5 clusters on other sites appear at 1000 K, increase up to about 40% of the total initial number at 1400 K, when there are almost no regular clusters anymore. Then these other I^5 clusters also vanish. Eye inspection of the atomic structures during these simulations shows that I^5 clusters disappear by the emission of one or more oxygen atoms, which destroy the cuboctahedral cluster. Oxygen atoms emitted from I^5 clusters tend to diffuse and some of them gather on other sites to again form five-atom clusters. Starting from 1000 K, I^5 clusters appear and disappear during the 50 ps simulated time, with decreasing lifetimes with increasing temperature. This makes the previous structural characterizations, based on time averaging, impossible to perform. Smaller clusters formed either by the destruction of I^5 clusters or gathering of emitted interstitials tend to evolve quickly and to be short-lived, with no specific structure.

Starting at 1400 K, no clusters are detected in the initial U_4O_9 positions anymore. The remaining I^5 clusters are formed on other sites. One may wonder whether U_4O_9 is formed again dynamically with I^5 clusters respecting the intercluster arrangements of U_4O_9 but on sites different from the original ones. To check this possibility we plotted the I^5–I^5 $g(r)$, see Fig. 10. In practice, clusters are located at the position of their central atom. At low temperatures, the $g(r)$ function exhibits distribution of peaks characteristic of U_4O_9 with the first peak at 1.87 $a_0 = 1/2(321)a_0$. All peaks remain visible up to 1200 K, where they rapidly disappear to form a flat signal at 1400 K, indicating that the U_4O_9 of I^5 clusters is not rebuilt at higher temperatures. One notes, however, that a minimal distance corresponding to the original first-neighbor distance (1.87 a_0) remains. I^5 clusters thus tend to repel each other at short distances.

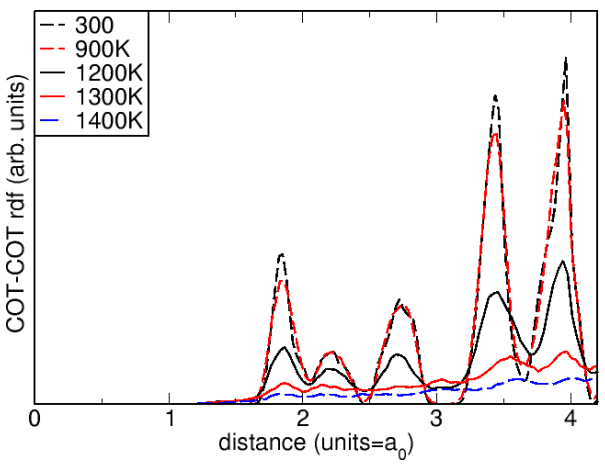

FIG. 10. I^5–I^5 radial distribution function $g(r)$ as a function of temperature. Results are reported in units of the equilibrium lattice constant a_0 that varies with the temperature.

IV. DISCUSSION

The search for the true ground-state structure of U_4O_9 at 0 K unexpectedly proved to be a formidable task. As detailed in Sec. II, we obtained many different stable structures depending on the initial atomic arrangements in the oxygen clusters. The many different minima we find are of purely structural origin, as we do not expect multiple minima due to electronic trapping in our simulations. We confirmed this by performing calculations at 0 K with the SMTB-Q empirical potential, where we also found many different stable structures all quite close in energy, thus showing that the complicated energetic landscape of U_4O_9 is a genuine feature of I^5 oxygen clusters.

Unfortunately, as already mentioned above, the lowest energy structure we found [$U_4O_9(I^5_X)$] seems to contradict the experimental facts as it contains U^{6+} ions that are considered absent in experiments [30,31]. We suspect that this structure could be an artifact of the DFT+U approach. This nonphysical result may originate from the fact that in our simulations all uranium atoms are treated equivalently, irrespective of their valence. While this obviously should be the case in a pure DFT, the DFT+U scheme relies on a tuning parameter U. We chose the same parameter for all uranium atoms and fitted it on the electronic structure of UO_2, which contains only U^{4+}. The proper description of U^{5+} and U^{6+} in overstoichiometric uranium oxide would certainly require one to choose different values of U for the 5+ and 6+ valences. The stabilization in some of our structures of U^{6+} thus may originate in this improper value of U. Nevertheless, having the same U for all uranium enables the electronic minimization to position freely the U^{5+}(and unfortunately to create the U^{6+}) in the U_4O_9 structure, which is an advantage over calculations where a different U parameter is chosen for the different uranium valences. In such calculations, the positions of the U^{5+} have to be chosen by hand.

The $U_4O_9(I^5_C)$ structure contain only U^{4+} and U^{5+} ions. The positions of the U^{5+} ions are common to most structures with no U^{6+} and thus do not seem to depend on the slight differences in I^5_C structures. It is worth stressing again that, surprisingly, not all the U^{5+} are linked to the I^5_C clusters. Twenty four out of 60 are indeed located on uranium atoms in the fluorite structure away from the oxygen clusters. Only the six uranium facing the I^5_C along ⟨100⟩ directions are U^{5+}. This result is consistent with the suggestion made by Desgranges *et al.* [7], based on the observation of the distances between uranium situated along ⟨111⟩ directions from the cluster centers and their oxygen first neighbors. They found a distance of 2.61 Å while ours is 2.68 Å which is very close when our distance is further rescaled to the shorter experimental a_0 value (18.82 Å instead of 19.15 Å). This consistency is a strong support for our $U_4O_9(I^5_C)$ predicted structure.

We turn now to evolution of the U_4O_9 structure with temperature in our simulations and their possible connections with experimental knowledge. A hint of strong I^5-I^5 interactions appears in our finite temperature simulations. Indeed, when the I^5 clusters start to disappear from their original site and form again in other sites, they never get closer from each other than they were in the ordered structure, which evidences strong short-range repulsion between them. The evolution of the I^5 center shift and interatomic distances both point to the symmetrization of the cluster with temperature. This symmetrization is consistent with experimental observations. Indeed, the β structure is more symmetric than the α one (higher symmetry space group). Moreover, Cooper and Willis [5] gave refined positions for I^5 at 503 and 773 K. Careful examination of their internal parameters prove that the cluster center gets closer to the perfect position and that their distortions (though different from the ones we simulate) are smaller at higher temperatures.

α to β and β to γ phase transitions have been associated in literature [36] to changes in the $U^{4+}-U^{5+}$ distribution as shown by the changes in the electrical conductivity which increases at the transition. We cannot establish any connections between our MD simulations and such changes in valences, as our empirical potential does not include multiple valences. Still, we observe that the rhombohedral structure tends to become cubic at higher temperatures. Nevertheless, our DFT calculations are consistent with the possibility of a disorder in U^{4+} and U^{5+} positions at a relatively low temperature. Indeed, we find a formation energy for the disconnected polaron pair of 64 meV. This proves to be a very low energy, 740 K in equivalent temperature units. One can compare with the equivalent energy in UO_2, which is 1.64 eV according to our calculations. This can be easily explained considering uranium valences. In UO_2, forming a polaron pair amounts to creating a pair of U^{5+} and U^{3+}. This process is obviously costly in energy. Quite the opposite in U_4O_9, creating a polaron pair consists of changing a U^{4+} into a U^{5+} and vice versa, essentially simply inverting the valence of two ions. The very small cost of this inversion is consistent with the apparition of valence changes and disorder at low temperature in U_4O_9. Furthermore, the existence of U^{5+} ions disconnected from the I^5 clusters and low lying in the gap may have a positive impact on the electric conduction of U_4O_9, something one can relate to the larger electrical conductivity of U_4O_9 compared to that of UO_2 [37].

Returning to the atomic arrangements in U_4O_9, our results evidence the huge structural freedom that exists in this structure. At 0 K, we found 35 different structures within 5.4 eV of each other. This energy spread proves quite small when rescaled by the number of atoms in the simulation box. Indeed, 1 eV amounts to 0.9 eV per cluster, 0.18 eV per oxygen interstitial, or 1.3×10^{-2} eV/atom in the simulation box, i.e., about 150 K in equivalent temperature. The difference between the two quite different structures $U_4O_9(I^5_X)$ and $U_4O_9(I^5_C)$ is 1.05 eV or 30 K.

We thus have to humbly consider that the $U_4O_9(I^5_C)$ structure presented above is just our best guess for the ground state structure of U_4O_9. Any change in the computational framework may result in a different prediction for the lowest energy structure. However, many features remain common to most of the structures, namely, the localization of U^{5+} and the magnitude of the gap.

V. CONCLUSION

In the present paper, we performed a combination of DFT relaxation at 0 K and SMTB-Q empirical potential MD simulations at finite temperature and zero pressure on U_4O_9 to

explore the properties of the α, β, and γ phases. These calculations were extremely challenging due to the unit cell size (414 atoms) and the numerous structural metastable states that trap the geometrical relaxation.

The DFT calculations have resulted in many metastable structures, among which we have identified two interesting candidates. The $U_4O_9(I^5_X)$ is the absolute ground state of our numerical approach. It is based on I^5_X clusters that are pure predictions from DFT+U calculations [10] and have no experimental confirmation. This structure involves U^{6+} cations which have no experimental counterpart either [30,31]. Our second structure $U_4O_9(I^5_C)$ conforms better to experimental facts, however, at a slightly higher energy in DFT+U. As discussed above, the energy differences we observe are nevertheless very small when considering the size of the unit cell.

Then turning on the temperature using empirical potential, we observe some expected features: the increase of symmetry with temperature, the convergence from pseudocubic to cubic, the centering of I^5_C oxygen clusters. A striking fact is the persistent repulsion between neighboring oxygen clusters, which systematically favors the very peculiar $1/2\langle 123\rangle a_0$ minimal distance between first-nearest neighbors.

The DFT calculations finally demonstrate the very low energetical cost of polaron pairs in U_4O_9, which gives support to the experimental claim that the β to γ phase change is driven by polaron arrangements [36].

ACKNOWLEDGMENTS

Inspiring discussions with Guido Baldinozzi are acknowledged. This work was performed using HPC resources from GENCI-CCRT-TGCC (Grant No. 2022-096018).

[1] D. Bevan, I. Grey, and B. Willis, The crystal structure of $\beta-U_4O_9-y$, J. Solid State Chem. **61**, 1 (1986).
[2] B. Belbeoch, J. C. Boivineau, and P. Perio, Changements de structure de l'oxyde U_4O_9, J. Phys. Chem. Solids **28**, 1267 (1967).
[3] N. Keiji, Phase transitions of U_4O_9, J. Nucl. Mater. **51**, 126 (1974).
[4] K. Seta, T. Matsui, H. Inaba, and K. Naito, Heat capacity and electrical conductivity of non-stoichiometric U_4O_9-y from 300 to 1200 k, J. Nucl. Mater. **110**, 47 (1982).
[5] R. I. Cooper and B. T. M. Willis, Refinement of the structure of b-U_4O_9, Acta Crystallogr. **A60**, 322 (2004).
[6] L. Desgranges, G. Baldinozzi, G. Rousseau, J. C. Nièpce, and G. Calvarin, Neutron diffraction study of the in situ oxidation of UO_2, Inorg. Chem. **48**, 7585 (2009).
[7] L. Desgranges, G. Baldinozzi, D. Simeone, and H. E. Fischer, Structural changes in the local environment of uranium atoms in the three phases of U_4O_9, Inorg. Chem. **55**, 7485 (2016).
[8] A. Soulié, G. Baldinozzi, F. Garrido, and J.-P. Crocombette, Clusters of oxygen interstitials in UO_2+x and alpha-U_4O_9: Structure and arrangements, Inorg. Chem. **58**, 12678 (2019).
[9] D. A. Andersson, G. Baldinozzi, L. Desgranges, D. R. Conradson, and S. D. Conradson, Density functional theory calculations of UO_2 oxidation: Evolution of UO_2+x, U_4O_9-y, U_3O_7, and U_3O_8, Inorg. Chem. **52**, 2769 (2013).
[10] L. Yang and B. D. Wirth, Clustering of excess oxygen in uranium dioxide: A first-principles study, J. Nucl. Mater. **554**, 153087 (2021).
[11] A. I. Liechtenstein, V. I. Anisimov, and J. Zaanen, Density-functional theory and strong interactions: Orbital ordering in Mott-Hubbard insulators, Phys. Rev. B **52**, R5467 (1995).
[12] S. L. Dudarev, G. A. Botton, S. Y. Savrasov, C. J. Humphreys, and A. P. Sutton, Electron-energy-loss spectra and the structural stability of nickel oxide: An LSDA+U study, Phys. Rev. B **57**, 1505 (1998).
[13] M. Cococcioni and S. de Gironcoli, Linear response approach to the calculation of the effective interaction parameters in the LDA+U method, Phys. Rev. B **71**, 035105 (2005).
[14] F. Aryasetiawan, K. Karlsson, O. Jepsen, and U. Schönberger, Calculations of Hubbard U from first-principles, Phys. Rev. B **74**, 125106 (2006).
[15] B. Amadon, T. Applencourt, and F. Bruneval, Screened coulomb interaction calculations: cRPA implementation and applications to dynamical screening and self-consistency in uranium dioxide and cerium, Phys. Rev. B **89**, 125110 (2014).
[16] G. Kresse and J. Furthmüller, Efficient iterative schemes for *ab initio* total-energy calculations using a plane-wave basis set, Phys. Rev. B **54**, 11169 (1996).
[17] J. P. Perdew, K. Burke, and M. Ernzerhof, Generalized Gradient Approximation Made Simple, Phys. Rev. Lett. **77**, 3865 (1996).
[18] F. Bruneval, M. Freyss, and J.-P. Crocombette, Lattice constant in nonstoichiometric uranium dioxide from first principles, Phys. Rev. Mater. **2**, 023801 (2018).
[19] R. Laskowski, G. K. H. Madsen, P. Blaha, and K. Schwarz, Magnetic structure and electric-field gradients of uranium dioxide: An *ab initio* study, Phys. Rev. B **69**, 140408(R) (2004).
[20] B. Dorado, B. Amadon, M. Freyss, and M. Bertolus, DFT + U calculations of the ground state and metastable states of uranium dioxide, Phys. Rev. B **79**, 235125 (2009).
[21] B. Dorado, M. Freyss, B. Amadon, M. Bertolus, G. Jomard, and P. Garcia, Advances in first-principles modelling of point defects in UO_2: f electron correlations and the issue of local energy minima, J. Phys.: Condens. Matter **25**, 333201 (2013).
[22] A. Soulié, F. Bruneval, M. C. Marinica, S. Murphy, and J. P. Crocombette, Influence of vibrational entropy on the concentrations of oxygen interstitial clusters and uranium vacancies in nonstoichiometric UO_2, Phys. Rev. Mater. **2**, 083607 (2018).
[23] G. Kresse and D. Joubert, From ultrasoft pseudopotentials to the projector augmented-wave method, Phys. Rev. B **59**, 1758 (1999).
[24] I. I. Kapshukov, N. V. Lyalyushkin, L. V. Sudakov, A. S. Bevz, and O. V. Skiba, Preparation of hypostoichiometric UO_{2-x} at low temperatures and study of some properties, J. Radioanal. Nucl. Chem. Artic. **143**, 213 (1990).
[25] J. Schoenes, Optical properties and electronic structure of UO_2, J. Appl. Phys. **49**, 1463 (1978).

[26] G. Leinders, G. Baldinozzi, C. Ritter, R. Saniz, I. Arts, D. Lamoen, and M. Verwerft, Charge localization and magnetic correlations in the refined structure of U_3O_7, Inorg. Chem. **60**, 10550 (2021).

[27] A. R. Oganov, C. J. Pickard, Q. Zhu, and R. J. Needs, Structure prediction drives materials discovery, Nat. Rev. Mater. **4**, 331 (2019).

[28] L. Desgranges, G. Baldinozzi, D. Siméone, and H. E. Fischer, Refinement of the alpha-U_4O_9 crystalline structure: New insight into the $U_4O_9 \rightarrow U_3O_8$ transformation, Inorg. Chem. **50**, 6146 (2011).

[29] See Supplemental Material at http://link.aps.org/supplemental/10.1103/PhysRevMaterials.7.063602 for the crystal structure, atomic positions, and pair correlation functions of the two studied structures for U_4O_9.

[30] K. O. Kvashnina, S. M. Butorin, P. Martin, and P. Glatzel, Chemical State of Complex Uranium Oxides, Phys. Rev. Lett. **111**, 253002 (2013).

[31] G. Leinders, R. Bes, K. O. Kvashnina, and M. Verwerft, Local structure in U(IV) and U(V) environments: The case of U_3O_7, Inorg. Chem. **59**, 4576 (2020).

[32] C. Freysoldt, B. Grabowski, T. Hickel, J. Neugebauer, G. Kresse, A. Janotti, and C. G. Van de Walle, First-principles calculations for point defects in solids, Rev. Mod. Phys. **86**, 253 (2014).

[33] A. Hallil, R. Tetot, F. Berthier, I. Braems, and J. Creuze, Use of a variable-charge interatomic potential for atomistic simulations of bulk, oxygen vacancies, and surfaces of rutile TiO_2, Phys. Rev. B **73**, 165406 (2006).

[34] N. Salles, O. Politano, E. Amzallag, and R. Tétot, Molecular dynamics study of high-pressure alumina polymorphs with a tight-binding variable-charge model, Comput. Mater. Sci. **111**, 181 (2016).

[35] A. Soulié, J.-P. Crocombette, A. Kraych, F. Garrido, G. Sattonnay, and E. Clouet, Atomistically-informed thermal glide model for edge dislocations in uranium dioxide, Acta Mater. **150**, 248 (2018).

[36] K. Naito, T. Tsuji, and T. Matsui, An electrical conductivity and x-ray study of a high-temperature transition in U_4O_9, J. Nucl. Mater. **48**, 58 (1973).

[37] J. Tateno and K. Naito, On the dielectric properties of U_4O_9 and UO_2, Solid State Commun. **7**, 807 (1969).